PCCP

ROYAL SOCIETY OF CHEMISTRY

COMMUNICATION

View Article Online
View Journal | View Issue

Cite this: *Phys. Chem. Chem. Phys.*, 2024, **26**, 17467

Received 1st December 2023,
Accepted 22nd May 2024

DOI: 10.1039/d3cp05857c

rsc.li/pccp

Probing of nucleic acid compaction using low-frequency Raman spectroscopy†

Andrey Yu. Sosorev, *[abc] Olga D. Parashchuk, [a] Ivan V. Chicherin,[d] Artem A. Trubitsyn,[a] Vasiliy A. Trukhanov, [a] Maria V. Baleva,[d] Ulyana E. Piunova,[d] Oleg G. Kharlanov, [a] Piotr Kamenski[d] and Dmitry Yu. Paraschuk [a]

Compaction of nucleic acids, namely DNA and RNA, determines their functions and involvement in vital cell processes including transcription, replication, DNA repair and translation. However, experimental probing of the compaction of nucleic acids is not straightforward. In this study, we suggest an approach for this probing using low-frequency Raman spectroscopy. Specifically, we show theoretically, computationally and experimentally the quantifiable correlation between the low-frequency Raman intensity from nucleic acids, magnitude of thermal fluctuations of atomic positions, and the compaction state of biomolecules. Noteworthily, we highlight that the LF Raman intensity differs by an order of magnitude for different samples of DNA, and even for the same sample in the course of long-term storage. The feasibility of the approach is further shown by assessment of the DNA compaction in the nuclei of plant cells. We anticipate that the suggested approach will enlighten compaction of nucleic acids and their dynamics during the key processes of the cell life cycle and under various factors, facilitating advancement of molecular biology and medicine.

Nucleic acids, namely DNA and RNA, are at the heart of biochemical processes in cells.[1] The emerging evidence suggests that the compaction of nucleic acids (NAs) – tightness of nucleotide packing resulting in constraints on their thermal motion – governs the key pathways of gene expression and genome maintenance, including transcription, translation, replication, recombination and DNA repair. Specifically, chromatin – DNA complexed with histone proteins – is present in the cell nucleus in the form of functionally different euchromatin and heterochromatin depending on its compaction degree. Compact heterochromatin is transcriptionally silent, whereas euchromatin is rich in genes and has an open structure easily accessible to DNA-binding enzymes implementing transcription, replication and remodeling.[2] Epigenetic changes in response to various factors result in rearrangements of chromatin, turning the transition between euchromatin and heterochromatin, and providing fine tuning of gene expression and cell proliferation.[3] Compaction of RNA is important as well: for instance, that of ribosomal RNA (rRNA), which constitutes the bulk of the ribosome, is essential for protein synthesis. Thus, detailed understanding of the NA (especially DNA) packing and dynamics, as well as their dependence on temperatures and other factors is of paramount importance for molecular biology and medicine. However, this understanding is far from being achieved. Unfortunately, the techniques for probing NA compaction and chromatin arrangement developed to date (*e.g.*, Hi-C,[4] neutron scattering,[5] X-ray scattering[6] and fluorescence labeling[7]) are hardly applicable for non-invasive *in vivo* studies.

A promising tool for studying the cell compartments, including nuclei, is Raman imaging microscopy.[8] Raman spectra of biomolecules in the high-frequency range (HF, the wavenumber above 200 cm^{-1}) typically contain characteristic bands corresponding to intramolecular vibrational modes. As a result, HF Raman spectra distinguish DNA, RNA, proteins and lipids so that HF Raman imaging can probe their distribution in cells,[8,9] as well as their dynamics, *e.g.*, during mitosis[10] and apoptosis.[11] Low-frequency (LF, below 200 cm^{-1}) Raman spectroscopy could provide invaluable information about the conformation of (bio)molecules and interactions between them, as LF spectra are associated with large-scale motions of extended molecular fragments controlled by non-covalent interactions. LF Raman spectra of biomolecules have been analyzed in a number of reports (see, *e.g.*, ref. 12–18). In a few of them, the nature and frequency of various LF bands were addressed for various DNA and RNA species under different conditions.[14–17] For instance, the effect of sequence[15] and humidity[14,16,17] was widely discussed. However, the *intensity* of LF Raman bands of NAs was

[a] *Faculty of Physics, Lomonosov Moscow State University, Leninskie Gory 1/62, Moscow 119991, Russia. E-mail: sosorev@physics.msu.ru*
[b] *Enikolopov Institute of Synthetic Polymeric Materials, Russian Academy of Sciences, Profsoyuznaya 70, Moscow 117393, Russia*
[c] *Shemyakin-Ovchinnikov Institute of Bioorganic Chemistry of the Russian Academy of Sciences, Ulitsa Miklukho-Maklaya, 16/10, Moscow 117997, Russia*
[d] *Faculty of Biology, Lomonosov Moscow State University, Leninskie Gory 1/12, Moscow 119234, Russia*

† Electronic supplementary information (ESI) available. See DOI: https://doi.org/10.1039/d3cp05857c

addressed only in a few reports,[13,14,17,18] and the analysis was nearly lacking in most of them.

On the other hand, we have recently shown that in another class of molecular materials, namely organic semiconductor crystals, high LF Raman intensities are observed for vibrations that strongly contribute to the dynamic disorder – thermally induced fluctuations of the positions and relative orientations of molecules.[19–22] Meanwhile, high HF Raman intensities underline vibrations that significantly affect the molecular polarizability, *i.e.*, contribute to local electron–phonon coupling.[23] Since measuring absolute LF Raman intensity is not straightforward, it is reasonable to use the ratio of LF Raman intensities to the HF ones (referred to as the R ratio in what follows), which provides a means for quantification and monitoring of the dynamic disorder in organic semiconductors.[20] In contrast to crystalline organic semiconductors, DNA and RNA are not periodic in the strict sense. However, in terms of solid-state physics, they can be regarded as systems with a strong static disorder, while extra disorder induced on top of it by thermal fluctuations at the picosecond timescale can be treated much like the dynamic disorder in molecular crystals. Note that such a definition of the dynamic disorder we adopt here excludes various motions at timescales longer than 10 ps and shorter than 0.1 ps: the former are related to slow conformational transitions of biomolecules, while the latter are associated with vibrations of chemical bonds (like the abovementioned intramolecular vibrations in molecular crystals). Between the two scales, however, there are vibrational modes that are thermally populated and are able to provide information about the molecular environment and compaction of the biomolecule.

In the current study, we formulate, test and apply a Raman-based approach to probe the dynamic disorder in NAs, thereby monitoring the compaction degree of these biomolecules. Unlike previous studies that used LF Raman spectra for analysis of the conformation of biomolecules, we focus on the relative LF Raman *intensity* instead of the frequencies of the bands, which allowed us to provide a quantitative estimate for the dynamic disorder. In the theoretical part, we introduce a version of the R ratio as a descriptor for the disorder in NAs and use molecular dynamics (MD) simulations to corroborate the connection between the disorder amplitude, the LF Raman spectrum and the compaction state of a biomolecule. Experimentally, we compare the R ratio for native and digested DNA and rRNA samples, and relate the observed difference to the degree of NA compaction therein. Furthermore, we report and explain a systematic decrease of the LF Raman intensity with long-term storage for DNA, whereas the rRNA spectrum changes slightly as assigned to the inherited compactified state of the ribosome. Accordingly, we argue that probing the dynamic disorder using a LF Raman-based technique enables monitoring the compaction of the NA molecules. Finally, we show that this monitoring can be performed *in vivo* using plant cells as an example.

To develop a spectroscopic descriptor of the dynamic disorder in NAs, we consider separately LF and HF Raman intensities. The Raman intensity is proportional to mean squared modulation of the polarizability tensor, α, of the

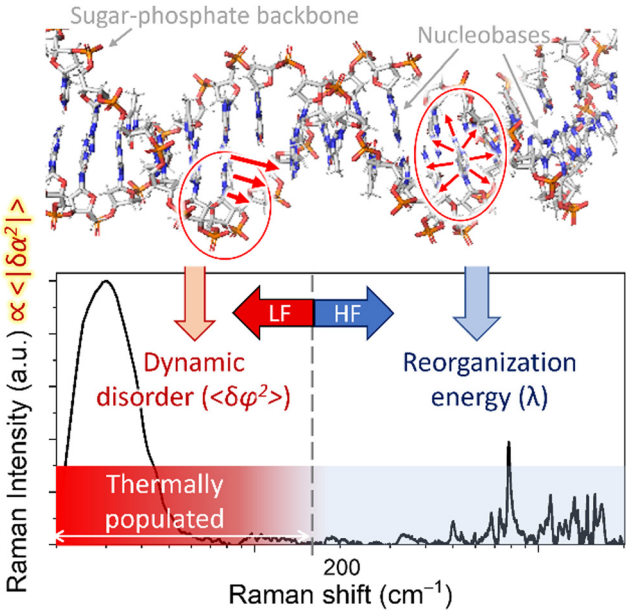

Fig. 1 Origins of LF and HF Raman signals for NAs.

system, $I \propto \langle \mathrm{tr}\delta\alpha^2(t)\rangle$ (see, *e.g.*, ref. 24). The LF Raman signal from NAs originates mainly from rotational vibrations (librations) of nucleosides[25] (see Fig. 1); in the latter, contributions of the nucleobases should dominate because of the much larger polarizability of the π-conjugated system of the nucleobase as compared to that of the non-conjugated (deoxy)ribose. Within the rigid-body approximation for the nucleobase librations, the tensor transformation law indicates that the vibrational modulation of the polarizability tensor for each nucleobase is proportional to the libration angle $\delta\varphi_n(t)$ around the instantaneous rotation axis, $\delta\alpha_n \sim \alpha_n\delta\varphi_n$, up to a factor of order unity. To arrive at the desired semiquantitative descriptor, we treat the polarizabilities α_n of individual nucleotides as being of the same order, denoted α_1 hereinafter, since they are rather comparable in reality (see, *e.g.*, our DFT estimations in Fig. S1, ESI†). For the whole biomolecule, the polarizability fluctuation thus reads $\delta\alpha \sim \alpha_1 \sum_n \delta\varphi_n$, and the LF Raman intensity is proportional to:

$$\int_{\mathrm{LF}} I\mathrm{d}\omega \sim CN_{\mathrm{res}}\alpha_1^2\sigma_\varphi^2 \cdot f \sim CN_{\mathrm{res}}\alpha_1^2\sigma_\varphi^2, \qquad (1)$$

where f is a factor describing correlations between the polarizability deviations for different nucleotides (which is of order unity, since the correlation length for vibrational modes is expected to be much smaller than the size of the biomolecule), C is a constant prefactor depending on the experimental conditions (pump intensity, active volume, *etc.*), and N_{res} is the number of nucleotides in the biomolecule. Finally, the quantity of interest σ_φ measures the characteristic angular amplitude of orientational disorder of the nucleobases, which can be regarded as a measure of the dynamic disorder in the whole NA molecule. In fact, the quantity $\alpha_1\sigma_\varphi$ on the right-hand side is nothing but the characteristic amplitude of the dynamic

polarizability disorder, *i.e.*, of thermal fluctuations of the nucleobase polarizabilities.

The HF Raman intensity (divided by the vibrational frequency) is related to the charge transfer reorganization energies of the nucleobases, λ_n.[21,23] To formulate a semiquantitative disorder descriptor, we stress that λ_n values are assumed to be close for various nucleobases. This is physically reasonable (see ref. 26); moreover, the percentages of various nucleotides in reasonably long native DNA and RNA samples are generally similar; therefore, the differences between λ values are effectively averaged out. As a result, the HF Raman intensity can be described as:

$$\int_{\mathrm{HF}} (I/\omega)\mathrm{d}\omega \sim C N_{\mathrm{res}} \alpha_1^2 \lambda_1, \qquad (2)$$

where C is the same constant as in eqn (1) and λ_1 is the average reorganization energy of one nucleobase. To eliminate the unknown C and N_{res} factors, we follow ref. 21 and introduce a spectroscopic quantity

$$R = \int_{\mathrm{LF}} I\mathrm{d}\omega \Big/ \int_{\mathrm{HF}} (I/\omega)\mathrm{d}\omega. \qquad (3)$$

Using eqn (1)–(3), we find

$$\sigma_\varphi \sim \sqrt{\lambda_1 R} \propto \sqrt{R}. \qquad (4)$$

Thus, a large R indicates strong dynamic disorder in NAs and can be used for its experimental assessment, in line with our results for organic semiconductors.[19–22]

It is natural to assign strong dynamic disorder (large R) to loose packing of the NA, *i.e.*, its weak compaction, so that large-scale nucleotide motions are possible. In contrast, in a densely packed (compacted) NA, large-scale nucleotide motion is hindered, resulting in a small R value. The following two factors seem to determine the compaction of NA: close packing of nucleotides within the helix and strong interaction between adjacent helices, so that both contribute to decrease of R. We emphasize that eqn (4) is only semiquantitative; however, in this study we show that R reasonably monitors the dynamic disorder and compaction of DNA and RNA.

To corroborate and illustrate our reasoning connecting the LF Raman intensity, dynamic disorder in different NA fragments (or nucleotides), and their molecular environment or compaction, we performed MD simulations of a linear DNA (27 nucleotide pairs, *i.e.*, N_{res} = 54 nucleotides) and of the ribosomal L1 stalk (N_{res} = 95), which are known for their important role in the translation process (see, *e.g.*, ref. 27), in explicit water solvent. Apart from their relative simplicity, these two structures were chosen because of their clearly different degrees of compaction (Fig. 2b and c): while the linear DNA maintains its quasi-1D structure with a uniform packing density, the L1 stalk exhibits a tertiary structure, which features fragments formed by relatively densely packed three and more RNA stems/loops. Fig. 2a shows LF Raman spectra predicted from 10 ns MD simulations of the two structures (see Methods for the computational protocol we used), after normalization to the numbers of nucleotides. Both spectra are represented by a LF wide-band background signal (LFWBS) and a number of bands on top of it (*e.g.*, those around 70–80 cm^{-1}, see inset in Fig. 2a). It is natural to assign this LFWBS to localized stochastic vibrations of the rather soft, nearly amorphous DNA structure with a lot of degrees of freedom.[28] The LF spectra, virtually characterizing the frequency distribution of the dynamic polarizability disorder for DNA and RNA, reveal a vivid difference: in the more compacted L1 stalk, the disorder is more shifted toward higher frequencies than in linear DNA. Moreover, the total root-mean-squared (RMS) disorder amplitude, after a "statistically inspired" normalization to $\sqrt{N_{\mathrm{res}}}$, turns out to be 30% smaller in L1 stalk than in DNA (see the bar chart in the inset in Fig. 2a). Furthermore, Fig. 2b and c evidences that, quite naturally, unpaired and terminal nucleotides are the "hot spots" with the highest disorder amplitudes, whereas those lying inside the quasi-3D compaction domains of L1 stalk are the least "noisy" (represented by bluish color shades in the figure). In contrast, all the nonterminal nucleotides in DNA are

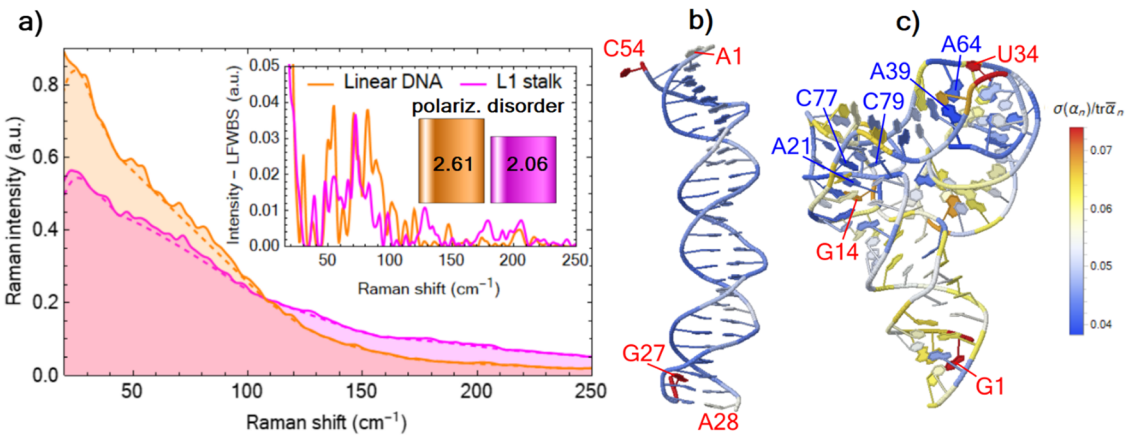

Fig. 2 (a) Calculated LF Raman spectra of a linear DNA and the ribosomal L1 stalk. The inset presents the spectra after subtraction of the LFWBS contribution to the spectrum, whose estimate is shown using a dashed curve in the main plot. The inset also presents the normalized RMS dynamic polarizability disorder amplitude, $\sigma_\alpha/\sqrt{N_{\mathrm{res}}}$, for the two molecules, in Å^3. (b) and (c) Structures of DNA (b) and L1 stalk (c), colored according to the relative polarizability disorder $\sigma(\alpha_n)/\mathrm{tr}\bar{\alpha}_n$ of individual nucleobases n. The "hot" and "cold" spots with the highest and lowest disorder are marked explicitly.

characterized with roughly the same disorder. A similar conclusion can be drawn from the RMS coordinate deviation analysis: over a 2 ns time window, this disorder metric is 2.7 Å for DNA atoms, compared with 1.5 Å for a more ordered L1 stalk (for details, see Section S1, in particular, Fig. S2, ESI†). Note that the L1 stalk is relatively soft compared with the ribosome as a whole (which strongly exceeded our simulation capabilities), so that the dynamic disorder for the latter is expected to be even lower. Thus, our MD results corroborate the formulated approach for LF Raman probing of dynamic disorder in NAs and their compaction.

We now move to the experimental Raman data for DNA and RNA samples. Fig. 3a presents the spectra for precipitated native (supercoiled) and digested (cut with DNAse I) DNA (semi)dry films. For the digested species, the cuts in one or both DNA strands prevent supercoiling and enable the relaxed (extended) conformation.[29] Since the experiments were performed in films, neighboring molecules interact with each other, and the digested DNA can pack in a more compact state than the supercoiled native one. The HF Raman spectra for both DNA species are typical for DNA[30] and exhibit prominent characteristic bands. These bands have similar frequencies and slightly different intensities for the two samples; their assignment with the corresponding intensity analysis is given in Section S4, ESI.†

The LF Raman spectrum of both DNA species (see Fig. 3a) is presented by relatively narrow bands above the LFWBS, in line with the earlier experimental[14–18] and computational data.[18,28] Note that since the experiments on DNA and RNA samples were performed for (semi)dry films, direct contribution of retained water to LFWBS is expected to be insignificant. The LFWBS contributes to the overall disorder[18] and hence should be accounted for to assess the latter *via* the R calculation. However, for investigation of the coherent vibrations (which reveal themselves as narrow bands) of biomolecules the LFWBS should be subtracted; thus, we will also use another descriptor, R', calculated without the LFWBS. The calculated R and R' values for the DNA samples studied are listed in Table 1. In the digested DNA, the LF signal is less intensive, resulting in a lower R value. After the subtraction of the LFWBS (inset of Fig. 3a), the difference in the LF spectrum between the native and digested DNAs remains prominent: the intensity of the lowest-frequency Raman band at $\sim$20 cm^{-1} is about 10 times higher for the native DNA than that for digested one, resulting in a much lower R' value corroborating the weaker dynamic disorder in the digested DNA. This decrease in LF Raman intensity resembles that observed with cooling (see Fig. S3, ESI†), which freezes molecular motion and hence dynamic disorder. The weaker disorder in the film of digested DNA

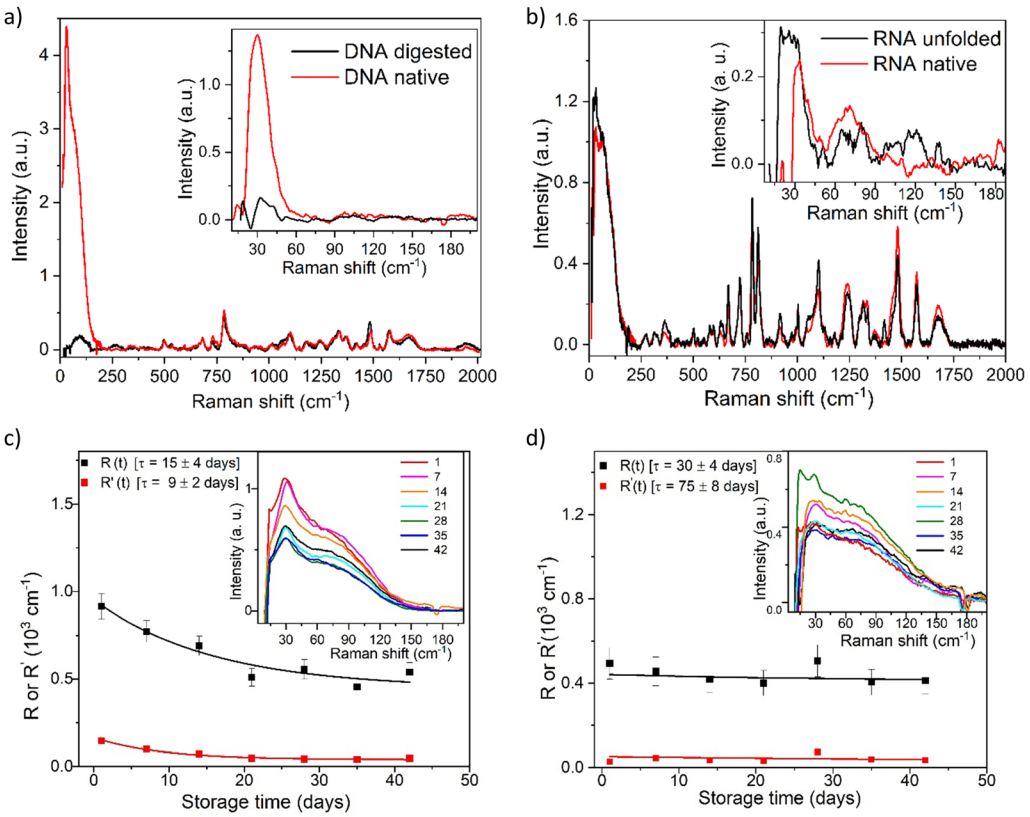

Fig. 3 (a) Raman spectra of native (red) and digested (black) DNA. (b) Raman spectra of native (red) and EDTA-treated (black) ribosome (rRNA). The spectra are normalized to the integrated HF intensity. The insets show the LF region with LFWBS subtracted. (c) and (d) Time dependence of R and R' for the native DNA (c) and ribosome (d). Lines are exponential fits ($R = A_1\exp(-t/\tau) + y_0$), with τ (in days) labeled on the graphs. The insets show the Raman spectra in the LF region with LFWBS, with the numbers of storage days given in the legends.

Table 1 R (R') values for the DNA and RNA samples, in cm^{-1}

NA	Native	Digested (DNA) EDTA-treated (RNA)
DNA	3818 (329)	131 (38)
RNA	1218 (91)	1230 (102)

can be ascribed to tighter packing of DNA helices or closer packing of nucleotides within the helices in this sample, as mentioned above. The tighter packing of the helices of digested DNA in films is corroborated by atomic-force microscopy data: while the native DNA precipitates from solution as extended isolated molecules, the digested DNA form aggregates (Section S5, ESI†). In addition, the decrease of dynamic disorder can have a contribution from changes in the helix conformation. Native DNA exists in the B-form of the helix, whereas digestion of the former can induce transition into other forms, *e.g.* A-form. This hypothesis is corroborated by emergence of the band at $\sim$807 cm^{-1} (characteristic for A-form[30,31]) and decrease of the band at $\sim$835 cm^{-1} (characteristic for B-form) in the digested DNA, as well as a shift of the band at $\sim$1421 cm^{-1} (see Fig. S4, ESI†). In the A-form, nucleobases are closer to each other than in the B-form: the interplane distance between adjacent nucleotides in the stack is $\sim$2.6 Å for A-form but $\sim$3.4 Å for B-form.[32] Closer stacking of nucleobases should hinder their relative motion and hence decrease their vibrational amplitudes, making the helix more rigid,[32] *i.e.* weakening the dynamic disorder. Thus, the decrease of R for the digested DNA can be partially attributed to the B- to A-form transition upon digestion. Note that contributions to compaction originating from B-to-A-form transition (intrahelical) and from strengthening interaction of helices (interhelical) could be entangled: different DNA helices of A-form DNA interact stronger than those of B-form DNA.[33] Disentangling of these contributions to R decrease is a subject of separate study.

We now focus on the ''sister molecule'' of the DNA, namely RNA, and measure Raman spectra for a ribosome – the nanomachine composed mainly ($\sim$2/3 by weight) of rRNA. Fig. 3b presents these spectra for native ribosomes and those treated with ethylenediaminetetraacetic acid (EDTA), which chelates magnesium ions extracting them from the ribosome and fostering the unfolding of the rRNA. As a result, the EDTA-treated ribosome is expected to be more loosely packed than the native ribosome, in which the magnesium ions support strong interaction between the rRNA helices.[34] The HF spectrum for both samples is typical for RNA[35] and close to that of DNA (*cf.* Fig. 3a and b). The LF Raman spectrum for both native and EDTA-treated ribosomes (both LFWBS-subtracted and non-subtracted) is significantly weaker than that for the native DNA (*cf.* Fig. 3a and b), in line with ref. 18. Correspondingly, the ribosomes show much lower R and R' values than the native DNA. This is in line with the much tighter and more ordered conformation of rRNA as compared to native DNA: the helices within a single ribosome are naturally assembled to form a relatively rigid structure.[34] Note that RNA exists in the A-form of the helix, which should have much weaker disorder than B-form (see above). The EDTA-treated ribosomes show the slightly stronger LFWBS and the lowest-frequency band than the native ones (albeit much weaker than the native DNA) resulting in slightly larger R and R', which are in line with a less compact character of the EDTA-treated ribosomes. Thus, our results for two DNA and two RNA samples highlight the feasibility of using R to probe the degree of dynamic disorder and compaction of NAs.

We also monitored the Raman spectra for another sample series of precipitated native DNA and ribosomes in the course of their long-term storage. Fig. 3c and d presents the corresponding $R(t)$ dependencies; the full recorded spectra are shown in Fig. S5, ESI.† Note that the samples for these studies potentially could have been prepared under slightly different conditions (*e.g.*, due to seasonal variations of the air temperature and humidity) compared to the samples described above. For this reason, the values of R/R' observed in the first day, $R(1)$, in Fig. 3c and d differ from those in Table 1; however, in both cases, R for the DNA is higher than the one for the ribosomes, in accordance with the more compact ribosome structure. Fig. 3c shows that LF Raman intensity of DNA significantly decreases with time so that R (R') drops by $\sim$2 (3) times in 40 days. We attribute this drop to suppression of the dynamic disorder in the sample due to the increase of the compaction degree: the remaining water evaporates from it during the storage time, and, as a result, the chains interact stronger. In addition, evaporation of the solvent can induce the transition from the B-form of the helix observed in native DNA to the A-form,[17] which is more compact and shows weaker dynamic disorder (see above). The latter hypothesis is corroborated by the emergence of a weak HF Raman band at 807 cm^{-1}, which is characteristic of the A-form, with time (Fig. S4a and c, ESI†). As mentioned above, the interhelical and intrahelical contribution to R decrease can be interdependent. The decrease of R with time is in accordance with the earlier observations that reported a drop in the LF Raman intensity,[17] and the THz signal in the range below 40 cm^{-1} [36] with a decrease in the air humidity. Our results are also in line with neutron scattering data showing a decrease in the RMS displacement of atoms with DNA drying[37] and shortening of the distance between the helices of the supercoiled DNA molecule with the increase of DNA concentration.[38] In contrast to DNA, the LF Raman intensity for the ribosome only slightly decreases after 40 days (see Fig. 3d), in accordance with its inherently tightly packed structure that is expected to be slightly affected by the neighboring ribosomes during drying. Moreover, rRNA in ribosomes is already in the A-form, and hence solvent evaporation does not induce crossover to the latter. These results corroborate the feasibility of the proposed approach for assessment of NA compaction and tracking dynamics of the latter. Note that $R(1)$ and τ are expected to depend on the sample preparation and storage conditions, *e.g.*, on temperature and air humidity, and are to be considered as estimates. However, we expect that for a given 'batch' of the DNA and ribosome samples, τ should be smaller for the former.

To address the potential of our approach to monitoring the compaction state *in vivo*, we recorded Raman spectra from the

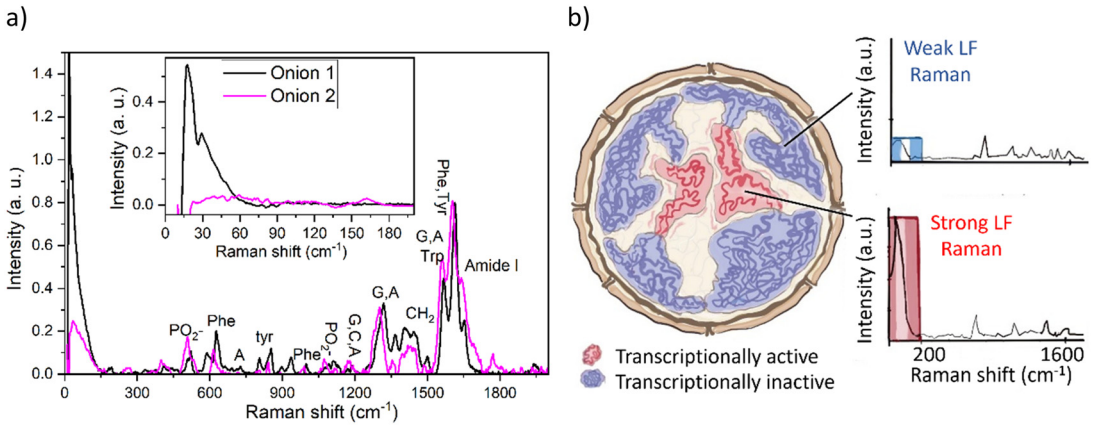

Fig. 4 (a) Raman spectra of onion nuclei. The inset shows the LF regions with LFWBS subtracted. (b) General idea of the monitoring DNA compaction using Raman microscopy.

two nuclei of plant (onion) cells; Fig. 4a shows these spectra. The HF parts of the spectra are quite similar, given that these spectra belong to the nuclei of different cells from different samples, and exhibit several characteristic peaks of DNA; note that some of them differ from those of the pristine DNA because of interaction with the proteins (see Section S4, ESI†). The LF Raman spectra for nuclei are weaker than that for the native DNA (see above). This can be tentatively ascribed to the more compact DNA in nuclei in comparison with the precipitated supercoiled DNA. Noteworthily, the LF spectrum for one nucleus shows a much larger intensity than that for the other, and this is a sign that the former nucleus (or, more probably, its probed area) contains more euchromatin.

The results presented above pave the way to noninvasive monitoring of the DNA compaction and its dynamics in nuclei of (living) cells. Fig. 4b illustrates the underlying idea of such monitoring. Raman spectra are measured in different points of the nucleus, like in conventional (HF) Raman imaging. The HF spectrum is nearly independent of DNA compaction and is used as a reference. In contrast, the LF spectrum is very sensitive to the compaction as shown above. Accordingly, the map of R values could indicate the areas exhibiting active transcription. Importantly, these areas can be monitored in living cells and in real time (*in vivo*), allowing tracing the effect of various factors (stress, mediators, and drugs) on the chromatin packing and dynamics. The approach can be extended to nonlinear Raman techniques, *e.g.*, CARS, improving the signal-to-noise ratio. The spatial resolution can also be improved by using advanced high-resolution optical microscopy techniques, *e.g.*, near-field scanning optical microscopy.

To conclude, we suggested a Raman-based approach for monitoring the compaction of NAs. Specifically, the connection between the dynamic disorder amplitude, the LF Raman intensity, and the compaction state of a biomolecule was established theoretically and corroborated computationally using MD, yielding the descriptor of NA compaction. The values of this descriptor calculated from the experimental data for various native and digested DNA and rRNA samples clearly correlate with the expected NA compaction in them. The descriptor also revealed the difference in the dynamics of DNA and rRNA compaction in the course of their long-term storage. Finally, the feasibility of the suggested approach for *in vivo* studies was shown using plant cells. We anticipate that our approach will shed light on the structure and dynamics of chromatin, as well as on their response to various factors, thereby advancing cell biology and finally areas of medicine such as oncology, histopathology, medical microbiology and immunology. Moreover, the suggested experimental tool for assessment of dynamic disorder at the nanoscale can be applied to other complex amorphous systems, providing new opportunities for physical chemistry.

Methods

Simulations of DNA and RNA and evaluation of their Raman spectra

LF Raman spectra of L1 stalk and linear DNA were calculated using a multiscale MD + DFT methodology:[18] instantaneous positions of nucleobases sampled from simulated MD trajectories were used for a fully-quantum (DFT) prediction of their polarizability tensors $\alpha_n(t)$, letting one obtain the spectra. In detail, the structures of L1 stalk and DNA from *E. coli* (RCSB PDB ref. codes 5ML7 and 6LXN, respectively[39]) were protonated, neutralized by Na^+ counterions, and solvated in water using AmberTools software.[40] The MD simulations which followed were based on AMBER force fields for nucleic acids: OL3 for L1 stalk and OL15 for linear DNA;[40] the water was described by the TIP3P model.[41] All simulations were performed in periodic boundary conditions. After energy minimization, 1.5-ns warmup to T = 300 K, and a further 4-ns equilibration at this temperature in the NPT ensemble, a production MD run followed with a total duration of 10 ns. Separately, for five methyl-terminated nucleobases n = A, C, G, T, and U, their equilibrium atomic positions $\mathbf{x}_{n,i}^{(0)}$, polarizability tensors $\alpha_n^{(0)}$ and derivatives $d\alpha_n^{(0)}/d\mathbf{x}_{n,i}$ were calculated in GAMESS US[42,43] at the B3LYP/6-31G(d,p) level of theory. Given these quantities (calculated only once) and instantaneous atomic coordinates $\mathbf{x}_{n,i}(t)$ for each nucleobase n each 50 fs of the MD simulation, an

in-house Python script evaluated the nucleobase polarizabilities on the fly using the formula $\alpha_n(t) = R_n(t)(\alpha_n^{(0)} + \mathrm{d}\alpha_n^{(0)}/\mathrm{d}\mathbf{x}_{n,i}\cdot\mathbf{r}_{n,i}(t))R_n^{\mathrm{T}}(t)$, featuring an orthogonal transformation $R_n(t)$ of the tensor and residual, non-rigid corrections. The non-rigid term was found from matching the MD geometries of the nucleobases with the equilibrium ones: $\mathbf{x}_{n,i}(t) = R_n(t)(\mathbf{x}_{n,i}^{(0)} + \mathbf{r}_{n,i}(t)) + \mathbf{\Delta}_n(t)$, where a rotation $R_n(t)$ and a rigid shift $\mathbf{\Delta}_n(t)$ form an isometry (see Section S1, ESI†). The polarizability $\alpha(t)$ of the whole structure (L1 stalk or DNA) was estimated as the sum of the polarizabilities of individual nucleobases therein. Once this was evaluated, the Raman spectrum was found as $I(\omega) \propto C(\omega)\cdot(\hbar\omega/k_{\mathrm{B}}T)\left(1 - e^{-\hbar\omega/k_{\mathrm{B}}T}\right)^{-1}$, where $C(\omega)$ is the Fourier transform of the polarizability autocorrelation function $\langle \mathrm{tr}(\delta\alpha(t)\delta\alpha(t+\tau))\rangle$, and the rest of the expression is the so-called detailed balance correction affecting frequencies around 200 cm^{-1} (see, *e.g.*, ref. 44). In principle, though we did not do this explicitly, one can use these spectra in eqn (3) to retrieve the R ratios (see Section S1, ESI†). The polarizability fluctuations were calculated as $\delta\alpha(t) = \alpha(t) - \bar{\alpha}(t)$, where $\bar{\alpha}(t)$ is a running mean over a 10-ps window. Finally, the RMS polarizability disorder is defined as $\sigma_\alpha = \langle \mathrm{tr}\delta\alpha^2(t)\rangle$, with angle brackets denoting a time average; the disorder for individual nucleobases, $\sigma(\alpha_n)$, was calculated analogously.

Preparation of biological samples

Plasmids pEGFP-N1 (Clontech, **https://www.addgene.org/vector-database/2491/**) and pTag-RFP-N (Evrogen, cat.# FP142) were isolated and purified with Plasmid Midiprep kit 2.0 (Evrogen, cat.# BC124) following the protocol from the supplier. The quality of the prepared plasmid DNA was controlled by electrophoresis in 1% agarose gel in a TBE buffer. The plasmid DNA was precipitated with ethanol, washed and air-dried for at least 30 minutes. Relaxed DNA was obtained by digestion of the plasmid with 0.5 U mg^{-1} DNase I for 30 minutes at 37 °C. The DNAse I treatment conditions were adjusted so that the enzyme introduced only single strand breaks and no more than one double strand break in the circular plasmid. Ribosomes were isolated from the *E. coli* strain MRE600 according to the protocol described earlier[45] (see Section S2, ESI†). The samples of "relaxed" ribosomes were prepared by chelating Mg^{2+} ions. For this, the samples collected after 15–40% sucrose gradient were diluted with at least four volumes of TE buffer (50 mM Tris–HCl pH 7, 10 mM EDTA) and collected by ultra-centrifugation. Several sets of DNA and ribosome samples were prepared, obtained in different time periods under slightly different conditions, *e.g.*, temperature and air humidity.

Raman spectroscopy

A Raman microscope (inVia, Renishaw) with a 50× objective lens (Leica DM 2500 M, NA = 0.75) equipped with a He–Ne laser (RL633, Renishaw) with a power of 17 mW was used. No signs of sample degradation were noted. The number of runs was chosen depending on the Raman signal intensity. All the spectra for the samples were measured at several points and then averaged to increase the single-to-noise ratio. The LF spectra were recorded in the confocal regime within the range of 10–450 cm^{-1} (series 1) with a built-in double monochromator (NExT, Renishaw). The notches in the LF spectra at 18, 25, and 160 cm^{-1} were artifacts caused by dust motes on the NExT filter mirrors. The HF Raman spectra were recorded in the confocal regime within the range of 100–1800 cm^{-1} (series 2) with Rayleigh edge filters. To reconstruct the Raman spectra covering both the LF and HF ranges, the corresponding spectra were stitched.[18] The details of spectrum processing are presented in Section S3, ESI.†

Conflicts of interest

There are no conflicts of interest to declare.

Acknowledgements

The study was supported by the MSU Program of Development, Grant # 23A-SCH04-02. The authors thank Evgeny Shirshin and Anna Rubekina (MSU) and Anton Chugunov (IBCh RAS) for fruitful discussions.

References

1 F. Crick, Central dogma of molecular biology, *Nature*, 1970, **227**, 561–563.
2 C. Alabert and A. Groth, Chromatin replication and epigenome maintenance, *Nat. Rev. Mol. Cell Biol.*, 2012, **13**, 153–167.
3 D. A. Stavreva and G. L. Hager, Chromatin structure and gene regulation: a dynamic view of enhancer function, *Nucleus*, 2015, **6**, 442–448.
4 E. Lieberman-Aiden, N. L. van Berkum, L. Williams, M. Imakaev, T. Ragoczy, A. Telling, I. Amit, B. R. Lajoie, P. J. Sabo and M. O. Dorschner, *et al.*, Comprehensive mapping of long-range interactions reveals folding principles of the human genome, *Science*, 2009, **326**, 289–293.
5 J. Ramón, V. Valencia, E. Tsimtsirakis, S. Krueger and A. Evilevitch, Temperature-induced DNA density transition in phage λ capsid revealed with contrast-matching SANS, *Proc. Natl. Acad. Sci. U. S. A.*, 2023, **120**(45), e2220518120.
6 C. Y. J. Hémonnot, C. Ranke, O. Saldanha, R. Graceffa, J. Hagemann and S. Köster, Following DNA Compaction During the Cell Cycle by X-ray Nanodiffraction, *ACS Nano*, 2016, **10**(12), 10661–10670.
7 J. Xu and Y. Liu, Probing Chromatin Compaction and Its Epigenetic States *in situ* With Single-Molecule Localization-Based Super-Resolution Microscopy, *Front. Cell Dev. Biol.*, 2021, **9**, 653077.
8 A. F. Palonpon, M. Sodeoka and K. Fujita, Molecular imaging of live cells by Raman microscopy, *Curr. Opin. Chem. Biol.*, 2013, **17**, 708–715.
9 I. W. Schie and T. Huser, Methods and Applications of Raman Microspectroscopy to Single-Cell Analysis, *Appl. Spectrosc.*, 2013, **67**, 813–828.
10 T. Guerenne-Del Ben, Z. Rajaofara and V. Couderc, *et al.*, Multiplex coherent anti-Stokes Raman scattering highlights state of chromatin condensation in CH region, *Sci. Rep.*, 2019, **9**, 13862.

11 O. Jonas, J. W. Kang, S. P. Singh, A. Lammers, F. T. Nguyen, R. R. Dasari, P. T. C. So, R. Langer and M. G. Cima, *In vivo* detection of drug-induced apoptosis in tumors using Raman spectroscopy, *Analyst*, 2018, **143**, 4836–4839.
12 B. S. Kalanoor, M. Ronen, Z. Oren, D. Gerber and Y. R. Tischler, New Method to Study the Vibrational Modes of Biomolecules in the Terahertz Range Based on a Single-Stage Raman Spectrometer, *ACS Omega*, 2017, **2**, 1232–1240.
13 V. S. Gorelik and A. Yu Pyatyshev, Raman Spectroscopy of DNA in a Wide Frequency Range, *Phys. Wave Phenom.*, 2014, **22**, 252–254.
14 H. Urabe and Y. Tominaga, Low-lying collective modes of DNA double helix by Raman spectroscopy, *Biopolymers*, 1982, **21**, 2477–2481.
15 O. P. Lamba, A. H. Wang and G. J. Thomas Jr, Low-frequency dynamics and Raman scattering of crystals, of B-, A-, and Z-DNA, and fibers of C-DNA, *Biopolymers*, 1989, **28**, 667–678.
16 C. Demarco, S. M. Lindsay, M. Pokorny, J. Powell and A. Rupprecht, Interhelical Effects on the Low-Frequency Modes and Phase Transitions of Li- and Na-DNA, *Biopolymers*, 1985, **24**, 2035–2040.
17 H. Urabe, Y. Sugawara, M. Ataka and A. Rupprecht, Low-Frequency Raman Spectra of Lysozyme Crystals and Oriented DNA Films: Dynamics of Crystal Water, *Biophys.*, 1998, **74**, 1533–1540.
18 A. Yu Sosorev, O. D. Parashchuk, O. G. Kharlanov, I. V. Chicherin, A. A. Trubitsyn, P. A. Kamenski and D. Yu Paraschuk, Low-Frequency Raman Scattering of Transfer and Ribosomal RNA, *JETP Lett.*, 2022, **116**, 335–341.
19 M. V. Vener, O. D. Parashchuk, O. G. Kharlanov, D. R. Maslennikov, D. I. Dominskiy, I. Y. Chernyshov, D. Y. Paraschuk and A. Y. Sosorev, Non-Local Electron-Phonon Interaction in Naphthalene Diimide Derivatives, its Experimental Probe and Impact on Charge-Carrier Mobility, *Adv. Electron. Mater.*, 2021, **7**, 2001281.
20 O. G. Kharlanov, D. R. Maslennikov, E. V. Feldman, G. G. Abashev, O. V. Borshchev, S. A. Ponomarenko, M. V. Vener, D. Y. Paraschuk and A. Y. Sosorev, Spectroscopic Assessment of Charge-Carrier Mobility in Crystalline Organic Semiconductors, *Adv. Electron. Mater.*, 2021, **7**, 2100579.
21 A. Yu Sosorev, O. D. Parashchuk, N. V. Tukachev, D. R. Maslennikov, D. I. Dominskiy, O. V. Borshchev, M. S. Polinskaya, M. S. Skorotetcky, O. G. Kharlanov and D. Yu Paraschuk, Suppression of dynamic disorder by electrostatic interactions in structurally close organic semiconductors, *Phys. Chem. Chem. Phys.*, 2021, **23**, 15485–15491.
22 A. Y. Sosorev, M. V. Vener, O. G. Kharlanov, E. V. Feldman, O. V. Borshchev, N. I. Sorokina, T. V. Rybalova, S. A. Ponomarenko and D. Y. Paraschuk, Efficient suppression of dynamic disorder in organic semiconductors via electron-donating and -withdrawing substituents, *J. Phys. Chem. C*, 2023, **127**, 17948–17957.
23 M. K. Nuraliev, O. D. Parashchuk, N. V. Tukachev, Y. A. Repeev, D. R. Maslennikov, O. V. Borshchev, Y. G. Vainer, D. Y. Paraschuk and A. Y. Sosorev, *J. Chem. Phys.*, 2020, **153**, 174303.
24 S. Y. Lee, Placzek-type polarizability tensors for Raman and resonance Raman scattering, *J. Chem. Phys.*, 1998, **78**, 723.
25 S. M. Perepelytsya and S. N. Volkov, Intensities of DNA ion-phosphate modes in the low-frequency Raman spectra, *Eur. Phys. J. E*, 2010, **31**, 201–205.
26 A. Yu Sosorev and O. G. Kharlanov, Organic nanoelectronics inside us: charge transport and localization in RNA could orchestrate ribosome operation, *Phys. Chem. Chem. Phys.*, 2021, **23**, 7037–7047.
27 S. Mohan and H. F. Noller, Recurring RNA structural motifs underlie the mechanics of L1 stalk movement, *Nat. Commun.*, 2017, **8**, 14285.
28 M. González-Jiménez, G. Ramakrishnan, N. V. Tukachev, H. M. Senn and K. Wynne, Low-frequency vibrational modes in G-quadruplexes reveal the mechanical properties of nucleic acids, *Phys. Chem. Chem. Phys.*, 2021, **23**, 13250–13260.
29 R. N. Irobalieva, J. M. Fogg, D. J. Catanese Jr., T. Sutthibutpong, M. Chen, A. K. Barker, S. J. Ludtke, S. A. Harris, M. F. Schmid, W. Chiu and L. Zechiedrich, Structural diversity of supercoiled DNA, *Nat. Commun.*, 2015, **6**, 8440.
30 G. J. Thomas Jr., J. M. Benevides and M. Tsuboi, *et al.*, Polarized Raman spectra of oriented fibers of A DNA and B DNA: anisotropic and isotropic local Raman tensors of base and backbone vibrations, *Biophys. J.*, 1995, **68**, 1073–1088.
31 J. M. Benevides, S. A. Overman and G. J. Thomas Jr., Raman, Polarized Raman and Ultraviolet Resonance Raman Spectroscopy of Nucleic Acids and Their Complexes, *J. Raman Spectrosc.*, 2005, **36**, 279–299.
32 D. W. Ussery, in DNA Structure: A-, B- and Z-DNA Helix Families, *Encyclopedia of life sciences*, Wiley, 2002.
33 L. Rudd, D. J. Lee and A. A. Kornyshev, The role of electrostatics in the B to A transition of DNA: from solution to assembly, *J. Phys.: Condens. Matt.*, 2007, **19**, 416103.
34 B. S. Schuwirth, *et al.*, Structures of the Bacterial Ribosome at 3.5 Å resolution, *Science*, 2005, **310**, 827–834.
35 A. J. Hobro, M. Rouhi, E. W. Blanch and G. L. Conn, *Nucleic Acids Res.*, 2007, **35**, 1169–1177.
36 A. Wittlin, L. Genzel, F. Kremer, S. Hiseler, A. Poglitsch and A. Rupprect, Far-infrared spectroscopy on oriented films of dry and hydrated DNA, *Phys. Rev. A*, 1986, **34**, 493.
37 E. Cornicchi, S. Capponi, M. Marconi, G. Onori and A. Paciaroni, Temperature dependence of fast fluctuations in single- and double-stranded DNA molecules. A neutron scattering investigation, *Philos. Mag.*, 2007, **87**, 509–515.
38 X. Zhu, S. Y. Ng and A. N. Gupta, *et al.*, Effect of crowding on the conformation of interwound DNA strands from neutron scattering measurements and Monte Carlo simulations, *Phys. Rev. E: Stat., Nonlinear, Soft Matter Phys.*, 2010, **81**, 061905.
39 H. M. Berman, J. Westbrook, Z. Feng, G. Gilliland, T. N. Bhat, H. Weissig, I. N. Shindyalov and P. E. Bourne, The Protein Data Bank, *Nucleic Acids Res.*, 2000, **28**, 235–242.
40 D. A. Case; K. Belfon; I. Y. Ben-Shalom; S. R. Brozell; D. S. Cerutti and T. E. Cheatham, (2020), AMBER 2020, University of California, San Francisco.

41 W. L. Jorgensen and J. D. Madura, Quantum and statistical mechanical studies of liquids. 25. Solvation and conformation of methanol in water, *J. Am. Chem. Soc.*, 1983, **105**, 1407–1413.
42 M. W. Schmidt, K. K. Baldridge, J. A. Boatz, S. T. Elbert, M. S. Gordon, J. H. Jensen, S. Koseki, N. Matsunaga, K. A. Nguyen and S. Su, *et al.*, General atomic and molecular electronic structure system, *J. Comput. Chem.*, 1993, **14**, 1347.
43 M. S. Gordon and M. W. Schmidt, in *Theory and applications of computational chemistry: the first forty years*, ed. C. E. Dykstra, G. Frenking, K. S. Kim and G. E.Scuseria, Elsevier, Amsterdam, 2005, p. 1167.
44 S. Luber, M. Iannuzzi and J. Hutter, Raman spectra from *ab initio* molecular dynamics and its application to liquid *S*-methyloxirane, *J. Chem. Phys.*, 2014, **141**, 094503.
45 S. Levitskii, K. Derbikova, M. V. Baleva, A. Kuzmenko, A. V. Golovin, I. Chicherin, I. A. Krasheninnikov and P. A. Kamenski, 60S dynamic state of bacterial ribosome is fixed by yeast mitochondrial initiation factor 3, *PeerJ*, 2018, **6**, e5620.